Available online at www.sciencedirect.com
ScienceDirect
Journal of Computational Physics 227 (2008) 7929–7951
JOURNAL OF COMPUTATIONAL PHYSICS
www.elsevier.com/locate/jcp

Simulation of fluid and particles flows: Asymptotic preserving schemes for bubbling and flowing regimes

José-Antonio Carrillo [a], Thierry Goudon [b,c,*], Pauline Lafitte [b,c]

[a] *ICREA and Departament de Matemàtiques, Universitat Autònoma de Barcelona, E-08193 Bellaterra, Spain*
[b] *Project-Team SIMPAF, INRIA Research Centre Lille–Nord Europe, Parc Scientifique de la Haute Borne, 40, Avenue Halley B.P. 70478, F-59658 Villeneuve d'Ascq Cedex, France*
[c] *Laboratoire Paul Painlevé, UMR 8524 CNRS, Université des Sciences et Technologies de Lille, Cité Scientifique, F-59655 Villeneuve d'Ascq Cedex, France*

Received 26 October 2007; received in revised form 29 April 2008; accepted 5 May 2008
Available online 13 May 2008

Abstract

In this work, we propose asymptotic preserving numerical schemes for the bubbling and flowing regimes of particles immersed in a fluid treated by two-phase flow models. The description comprises compressible Euler equations for the dense phase (fluid) and a kinetic Fokker–Planck equation for the disperse phase (particles) coupled through friction terms. We show numerical simulations in the relevant case of gravity in the one-dimensional case demonstrating the overall behavior of the schemes.

MSC: 76T10; 76T15; 76T20; 65M99; 82D05; 82C80

Keywords: Fluid/particle coupling; Splitting methods; Asymptotic preserving schemes; Pollutant modeling; Gravity/buoyancy dominated flows

1. Introduction

We are interested in the numerical simulation of models describing the time evolution of particle suspensions in flows. The fluid/particle mixture is described as a two-phase flow where we adopt a statistical viewpoint for the disperse phase (the particles), whereas we use the standard description from continuum mechanics for the dense phase (the fluid). Therefore, the basic models couple fluid with kinetic equations where the mean velocity is driven by the fluid velocity. This kind of fluid–particle interaction models has applications in several fields as the description of diesel engines [42,41,17,1], rocket propulsors [36], pollution

* Corresponding author. Address: Project-Team SIMPAF, INRIA Research Centre Lille–Nord Europe, Parc Scientifique de la Haute Borne, 40, Avenue Halley B.P. 70478, F-59658 Villeneuve d'Ascq Cedex, France. Fax: +33 320210776.
E-mail addresses: carrillo@mat.uab.es (J.-A. Carrillo), Thierry.Goudon@inria.fr (T. Goudon), pauline.lafitte@math.univ-lille1.fr (P. Lafitte).

0021-9991/$ - see front matter © 2008 Elsevier Inc. All rights reserved.
doi:10.1016/j.jcp.2008.05.002

settling processes [6,40], rain formation [18], chemical engineering, wastewater treatment [5] or biomedical flows [4].

Specifically, this work is devoted to the following system of partial differential equations, devised in [7]:

$$\begin{cases} \partial_t f + \beta\xi\cdot\nabla_x f - \eta'\nabla_x\Phi\cdot\nabla_\xi f = \frac{1}{\epsilon}\nabla_\xi\cdot\left(\left(\xi-\frac{1}{\beta}u\right)f+\nabla_\xi f\right), \\ \partial_t n + \mathrm{div}_x(nu) = 0, \\ \partial_t(nu) + \mathrm{Div}_x(nu\otimes u) + \nabla_x p(n) + \eta n\nabla_x\Phi = \frac{1}{\epsilon}\frac{\rho_P}{\rho_F}(J-\rho u), \end{cases} \tag{1}$$

where we use the notation

$$\rho(t,x) = \int_{\mathbb{R}^3} f(t,x,\xi)\mathrm{d}\xi, \quad J(t,x) = \beta\int_{\mathbb{R}^3}\xi f(t,x,\xi)\mathrm{d}\xi.$$

The disperse phase is described by its particle distribution function in the phase space $f(t,x,\xi)\geqslant 0$. The particles interact with a dense phase, described by its density $n(t,x)$, and its velocity field $u(t,x)$. As far as we are concerned with the description of modeling issues, we consider the three-dimension case: $t\geqslant 0$, $x\in\mathbb{R}^3$, $\xi\in\mathbb{R}^3$; whereas numerical simulations will be performed in the one-dimension framework. Both phases are subject to friction forces exerted by the other phase, proportional to the relative velocity $u(t,x)-\xi$, and also to external forces embodied into the potential Φ. We will be particularly interested in the case of gravity and buoyancy forces. Particles are also subject to a Brownian motion, that leads to a diffusion term with respect to the velocity variable, according to Einstein [16]. Here the system is written in a dimensionless form that makes the physical parameters β, ϵ, η and η' appear. By convention, all the parameters are positive but η' which can be either positive or negative: indeed, this indicates that the external forces might act differently on both phases, not only by strength but possibly also with opposite directions; this will be detailed below. We wish to design numerical schemes specifically dedicated to treat asymptotic regimes, in particular the limit $\epsilon\to 0$. For further purposes, it is convenient to introduce the shifted Fokker–Planck operator: for a given $u\in\mathbb{R}^3$, we set

$$L_u(f) = \nabla_\xi\cdot((\xi-u)f+\nabla_\xi f) = \nabla_\xi\cdot(M_u\nabla_\xi(f/M_u)), \quad M_u(\xi) = \frac{\mathrm{e}^{-|\xi-u|^2/2}}{(2\pi)^{3/2}}$$

and we will denote $L := L_0$, $M := M_0$. Accordingly, the penalized right hand side in the kinetic equation for the disperse phase in (1) reads $\frac{1}{\epsilon}L_{u(t,x)/\beta}(f)$ and we can expect for small ϵ's a relaxation to the Maxwellian $M_{u(t,x)/\beta}(\xi)$.

More details on the physical background can be found in [42] in connection to combustion phenomena. We mention the derivation of similar coupled models for disperse and dense phases in [27,28,20]. The question of "turbulence effects" on the disperse phase is addressed in [15,24]. Note that here we neglect collisional effects and size variations that could be important for some applications, see e.g. [3]. The analysis of a coupled model involving the incompressible Navier–Stokes system instead of the Euler equations is performed in [26]. Considering such a coupling, asymptotic problems were dealt with in [10,25,21,22]. A rigorous existence result for a coupling involving the compressible Navier–Stokes equations (which means that the dissipative term $\mu\Delta u$ is added in the fluid equation in (1)) is established in [37] while the analysis of its asymptotic limit is performed in [38]. The local well-posedness of smooth solutions for the system (1) was investigated in [2] while asymptotic problems and stability properties are studied in [7].

Here, we wish to investigate numerically the system (1) and the asymptotic regimes by proposing suitable asymptotic preserving schemes, in the sense introduced by Jin [29] (see the comments in Section 3). To this end, we shall use a fully explicit scheme, in the spirit of methods introduced for gas dynamics [33,32], neutron transport [30,31] or used in radiative transfer theory [23] and which were discussed recently in [8]. Splitting techniques for the kinetic part will be the basis to separate stiff parts from convection parts making some potentially troublesome terms with large velocities of order one. The flow part will be solved by state-of-the-art Lagrangian-projection schemes with anti-diffusive properties developed in [35,12–14,34,11].

Moreover, we numerically investigate two different asymptotic regimes in one of the most important cases of application in which particles (pollutants) inside the flow (air) are under the action of gravity and buoyancy

in one-dimension as considered e.g. in [5,40]. We will show the qualitative differences between the bubbling and the flowing regimes and the stability of sedimentation/buoyancy profiles in the bubbling regime as theoretically investigated in [7]. Furthermore, the chosen test cases will demonstrate the ability of the proposed numerical schemes to deal with strong shock situations, almost vacuum regions and concentrations of density.

The paper is organized as follows: in Section 2, we go back to the modeling issues, explaining the meaning of the dimensionless parameters and introducing the asymptotic problems we are interested in. In Section 3, we introduce the numerical scheme, detailing the steps of the splitting approach. Finally, we discuss our numerical results in Section 4.

2. Overview on modelling and asymptotic issues

2.1. Dimensionless parameters

System (1) is written in a dimensionless form; it involves the following parameters that are related to physical quantities (we refer to Carrillo and Goudon [7] for a detailed discussion on the scaling):

- ϵ is the ratio of the Stokes settling time $\frac{2\rho_P a^2}{9\mu}$ over the time scale of observation, a and ρ_P being the radius of the (supposedly spherically shaped) particles and their density, respectively, and μ being the dynamic viscosity of the fluid. This parameter, referred to as the Stokes number, measures the strength of the friction force.
- ρ_P/ρ_F is the ratio of the density of particles over the typical density of the surrounding gas.
- β is the ratio of the thermal velocity of the particles, which measures the fluctuation of particles velocities, over the typical velocity of the fluid.
- η' is, up to its sign, ϵ^{-1} times the ratio of the Stokes velocity, that enters into the scaling of the external forces, over the thermal velocity.
- η/η' describes how different the influence of the external forces is on the different phases; it is a dimensionless coefficient with a sign.

Gravity driven flows. It is worth illustrating this discussion with the example of gravity and buoyancy forces where the external potential is equal to gz, g being the gravitational acceleration and z the height direction. Then, the Stokes velocity is defined as $V_S = \frac{2\rho_P a^2}{9\mu} g|1 - \rho_F/\rho_P|$; it corresponds to the asymptotic velocity of a single particle with radius a and density ρ_P dropped in a viscous fluid at rest having dynamic viscosity μ. Accordingly, introducing time and length units, T and L, *respectively, we get*

$$\eta' = \frac{g(1-\rho_F/\rho_P)T}{\sqrt{k\Theta/m_P}},$$

where $m_P = \frac{4}{3}\pi a^3 \rho_P$, Θ is the temperature, k the Boltzmann constant. The sign of this parameter depends on the ratio ρ_F/ρ_P which accounts for the relative strength of the buoyancy and gravity forces. As said above, it can be rewritten as

$$|\eta'| = \frac{1}{\epsilon}\frac{V_S}{\sqrt{k\Theta/m_P}}.$$

Concerning the action of gravity on the fluid, we obtain the following expression for the dimensionless coefficient

$$\eta = \frac{gT}{U},$$

where $U = L/T$ measures the typical velocity of the fluid.

Therefore, in this context, $1/\sqrt{\eta}$ is the Froude number Fr_F of the flow, whereas $1/\sqrt{|\eta'|}$ is the (reduced) Froude number Fr_P of the disperse phase. We will be interested in the respective Richardson numbers, $Ri = 1/Fr^2$, of both phases. They characterize the effect of gravity over buoyancy, particularly used in aeronautics engineering, where it is considered as a rough measure of air turbulence. Thus, $Ri_F = \eta$ and

$Ri_P = |\eta'|$ and, being this number less/greater than unity means that the corresponding phase is gravity-driven/buoyancy dominated, respectively. Anyway, note that the previous definitions lead to

$$\frac{\eta'}{\eta} = (1 - \rho_F/\rho_P)\frac{1}{\beta}.$$

Density-dependent viscosity. From the modeling point of view, it may seem strange that the action of the friction forces is not negligible in regions where the density of the fluid is negligible. However, a usual assumption in compressible gases is to assume that the viscosity is temperature dependent. Even in pollution modeling, the air-viscosity is temperature dependent [40] and some models have been proposed like $\mu = C_0 T^{3/2}$, see [19]. In our chosen isentropic p-system, the equation of state is $n = (RT)^{1/(\gamma-1)}$, where R is the perfect gas constant and T is the temperature. We might assume that the viscosity is density-dependent as $\mu = \tilde{\mu} n^\alpha$ for a fixed $\alpha > 0$, and thus the dimensionless system reads as

$$\begin{cases} \partial_t f + \beta\xi \cdot \nabla_x f - \eta' \nabla_x \Phi \cdot \nabla_\xi f = \frac{n^\alpha}{\epsilon} \nabla_\xi \cdot \left(\left(\xi - \frac{1}{\beta} u \right) f + \nabla_\xi f \right), \\ \partial_t n + \mathrm{div}_x(nu) = 0, \\ \partial_t (nu) + \mathrm{Div}_x(nu \otimes u) + \nabla_x p(n) + \eta n \nabla_x \Phi = \frac{1}{\epsilon} \frac{\rho_P}{\rho_F} n^\alpha (J - \rho u), \end{cases} \tag{2}$$

where the dimensionless parameter ϵ is redefined accordingly. Other models assume from the beginning that the friction force depends on the fluid density, see for instance in [36] where the friction coefficient depends linearly on n.

Remark 1. Dealing with friction forces depending on the viscosity, but neglecting viscosity effects in the fluid equation might seem awkward from the modeling point of view. This is however often used in applications, especially in connection to combustion problems, and it leads to more challenging questions for numerics. Note that the Stokes number is related to the Reynolds number by $\epsilon = \frac{2}{9}(\rho_P/\rho_F)(a/L)^2 Re$ and $a \ll L$.

2.2. Dissipation properties and asymptotic regimes

We wish to investigate numerically (1), at least considering some asymptotic regimes. The starting point of the asymptotic analysis relies on the following dissipation property.

Proposition 1 (Entropy dissipation property). *We suppose that*

$$\frac{\rho_P}{\rho_F}\beta^2 = 1, \quad \eta' = \varsigma\beta, \quad \text{with } \varsigma = \pm 1. \tag{3}$$

Let us define the free energies associated, respectively, to the particles and to the fluid as follows:

$$\mathcal{F}_P(t) = \int_{\mathbb{R}^3} \int_{\mathbb{R}^3} \left(f \ln(f) + \frac{\xi^2}{2} f + \varsigma \Phi f \right) d\xi\, dx,$$

$$\mathcal{F}_F(t) = \int_{\mathbb{R}^3} \left(n \frac{|u|^2}{2} + \Pi(n) + \eta \Phi n \right) dx,$$

where $\Pi : \mathbb{R}^+ \to \mathbb{R}^+$ *is defined by* $s\Pi''(s) = p'(s)$. *Then, we have*:

$$\frac{d}{dt}(\mathcal{F}_P + \mathcal{F}_F) + \frac{1}{\epsilon} \int_{\mathbb{R}^3} \int_{\mathbb{R}^3} |(\xi - \beta^{-1}u)\sqrt{f} + 2\nabla_\xi \sqrt{f}|^2 \, d\xi\, dx \leqslant 0. \tag{4}$$

This statement is also valid under no-flux boundary conditions for the flow phase and reflection boundary conditions on the disperse phase for the kinetic distribution, see [7] for details. Assuming a power pressure law $p(n) = n^\gamma$, we have $\Pi(n) = n^\gamma/(\gamma - 1)$ for $\gamma > 1$ and $\Pi(n) = n \ln(n) - n$ for $\gamma = 1$. This claim helps in understanding the asymptotic regime $\epsilon \ll 1$: we infer that f has essentially a hydrodynamic behavior

$$f(t,x,\xi) \simeq \rho(t,x)\ (2\pi)^{-3/2} \exp(-|\xi - \beta^{-1}u(t,x)|^2/2) = \rho(t,x) M_{u(t,x)/\beta}(\xi).$$

Of course the evolution of the macroscopic density ρ remains to be discussed and highly depends on the other scaling assumptions. To be more specific, in [7], the following regimes are distinguished:

The bubbling regime. We set

$$\beta = \frac{1}{\sqrt{\epsilon}}, \quad |\eta'| = \frac{1}{\sqrt{\epsilon}}.$$

Coming back to the physical quantities, it means that

Stokes velocity $\simeq$ typical velocity of the fluid $\ll$ thermal velocity.

According to (3), we also have:

$$\frac{\rho_P}{\rho_F} = \epsilon,$$

and we suppose that η, which might depend on ϵ, tends to a positive constant $\eta_\star$.

The flowing regime. We assume that:

$$\beta^2 \frac{\rho_P}{\rho_F} = 1, \quad \beta = |\eta'| \text{ a fixed positive constant}$$

not depending on ϵ, as well as $\eta > 0$. Coming back to the physical quantities, this scaling assumption means

Stokes velocity $\ll$ typical velocity of the fluid $\simeq$ thermal velocity,

while the ratio ρ_P/ρ_F is of order β^{-2}.

Remark 2 (The gravity driven case). The scaling assumption (3) can be recast as

$$Ri_F = \eta = \frac{\beta^2}{|1-\beta^2|} \quad \text{and} \quad Ri_P = |\eta'| = \beta,$$

with $\varsigma = \mathrm{sgn}(1-\beta^2)$. Consequently, we have:

1. *In the bubbling regime*: *As* $\epsilon \to 0$, *we have* $\rho_P/\rho_F \ll 1$, $Ri_F \to 1$ *and* $\mathrm{Ri}_P \gg 1$; *thus, the disperse phase is buoyancy driven while the flow is gravity driven. Here* $\eta' < 0$ *and the external forces act in opposite directions on the particles and on the fluid, and we might expect the formation of sedimentation profiles at opposite ends.*
2. *In the flowing regime*: *We point out that* $\beta = \sqrt{\rho_F/\rho_P}$ *can take any* fixed value independent of $\epsilon \to 0$. Note $\beta = 1$ means we are dealing with a single phase flow. Having β close to 1 means that the effect of the external force on the disperse phase is very low. Taking into account the values of the Richardson numbers, we expect the following: when β is larger than 1, the forces act in opposite directions on both phases whereas when β becomes smaller than 1, the two phases are driven by gravity, but with more influence on the fluid.

For instance considering the application to rocket propulsors, we have $\rho_P/\rho_F \simeq 5.10^2$, see [36]; for fuel sprays a typical value is $\rho_P/\rho_F \simeq 34$, see [17], or for industrial thickening $\rho_P/\rho_F \simeq 2.5$, see [6].

2.3. Derivation of the limit equations

Let us derive formally the limit equations corresponding to the asymptotic regimes $\epsilon \to 0$ described above. From now on, according to (3), we use (1) where we set $\eta' = \varsigma\beta$, $\varsigma = \mathrm{sgn}(\eta')$ (which is -1 in the bubbling regime) and $\rho_P/\rho_F = 1/\beta^2$.

2.3.1. Bubbling regime

The bubbling regime can be readily understood by inserting the following Hilbert expansion

$$f_\epsilon = f^{(0)} + \sqrt{\epsilon} f^{(1)} + \epsilon f^{(2)} + \cdots \tag{5}$$

into (1) and identifying terms arising with similar power of $\sqrt{\epsilon}$. We get

- ϵ^{-1} terms: $Lf^{(0)} = 0$ which implies that $f^{(0)}(t,x,\xi) = \rho(t,x)M(\xi)$.

- $\epsilon^{-1/2}$ terms: $Lf^{(1)} = \xi \cdot \nabla_x f^{(0)} + (u + \nabla_x \Phi)\nabla_\xi f^{(0)} = \xi M(\xi)(\nabla_x \rho - (u + \nabla_x \Phi)\rho)$, where we used the fact that $\varsigma = \mathrm{sgn}(\eta') = -1$ in this regime. This equation can be readily inverted remarking that $L(\xi M(\xi)) = -\xi M(\xi)$; we obtain

$$f^{(1)}(t,x,\xi) = -\xi M(\xi)(\nabla_x \rho - (u + \nabla_x \Phi)\rho).$$

- ϵ^0 terms: $Lf^{(2)} = \partial_t f^{(0)} + \xi \cdot \nabla_x f^{(1)} + (u + \nabla_x \Phi) \cdot \nabla_\xi f^{(1)}$. However, $\int h \, \mathrm{d}\xi = 0$ appears as a necessary condition for the equation $L(f) = h$ to admit a solution. We are thus led to

$$\partial_t \left(\int_{\mathbb{R}^3} f^{(0)} \, \mathrm{d}\xi \right) + \mathrm{div}_x \left(\int_{\mathbb{R}^3} \xi f^{(1)} \, \mathrm{d}\xi \right) = \partial_t \rho - \nabla_x \cdot (\nabla_x \rho - (u + \nabla_x \Phi)\rho) = 0.$$

This so-called Smoluchowski equation is coupled to the Euler system whose right hand side is

$$\int_{\mathbb{R}^3} \left(\frac{\xi}{\sqrt{\epsilon}} - u \right) f \, \mathrm{d}\xi \simeq \int_{\mathbb{R}^3} \xi f^{(1)} \, \mathrm{d}\xi - u \int_{\mathbb{R}^3} f^{(0)} \, \mathrm{d}\xi = -(\nabla_x \rho - \rho \nabla_x \Phi).$$

We end up with the system

$$\begin{cases} \partial_t \rho + \mathrm{div}_x(\rho(u + \nabla_x \Phi) - \nabla_x \rho) = 0, \\ \partial_t n + \mathrm{div}_x(nu) = 0, \\ \partial_t (nu) + \mathrm{Div}_x(nu \otimes u) + \nabla_x(p(n) + \rho) + (\eta_\star n - \rho)\nabla_x \Phi = 0, \end{cases} \tag{6}$$

that was derived in [7] based on the moment system.

Remark 3. In the numerical simulations, we will complete the kinetic equation by the specular reflection boundary condition

$$f(t,x,\xi) = f(t,x,\xi - 2(\xi \cdot \nu(x))\nu(x)) \text{ for any } (x,\xi) \in \partial\Omega \times \mathbb{R}^N, \text{ such that } \xi \cdot \nu(x) < 0,$$

where $\nu(x)$ stands for the outer normal vector at the point $x \in \partial\Omega$. Obviously, this boundary condition guarantees mass conservation. Looking at the asymptotic problem, the leading term $f^{(0)}$ clearly satisfies the reflection boundary condition and we obtain relevant information by considering the corrector $f^{(1)}$. Imposing the reflection law leads to the following Robin condition

$$(\nabla_x \rho - (u + \nabla_x \Phi)\rho) \cdot \nu(x) = 0 \quad \text{on } \partial\Omega, \tag{7}$$

which completes (6) and also preserves mass for the limit system.

2.3.2. Flowing regime

Proceeding similarly for the flowing regime, we get

- ϵ^{-1} terms: $L_{u/\beta}(f^{(0)}) = 0$ and we infer that $f^{(0)}(t,x,\xi) = \rho(t,x)\, M_{u(t,x)/\beta}(\xi)$.
- ϵ^0 terms: $L_u(f^{(1)}) = \partial_t f^{(0)} + \xi \cdot \nabla_x f^{(0)} - \varsigma \nabla_x \Phi \cdot \nabla_\xi f^{(0)}$ and integration with respect to ξ yields the mass conservation

$$\partial_t \rho + \nabla_x \cdot (\rho u) = 0.$$

To describe the coupling, we remark that

$$\begin{aligned} &\frac{1}{\beta} \partial_t \left(\int_{\mathbb{R}^3} \xi f \, \mathrm{d}\xi \right) + \mathrm{Div}_x \left(\int_{\mathbb{R}^3} \xi \otimes \xi f \, \mathrm{d}\xi \right) + \varsigma \nabla_x \Phi \int_{\mathbb{R}^3} f \, \mathrm{d}\xi = -\frac{1}{\epsilon} \frac{1}{\beta^2} \int_{\mathbb{R}^3} (\beta\xi - u) f \, \mathrm{d}\xi \\ &\quad = -(\partial_t (nu) + \mathrm{Div}_x(nu \otimes u) + \nabla_x p(n) + \eta n \nabla_x \Phi). \end{aligned} \tag{8}$$

Therefore, at the leading order we obtain

$$\partial_t((n + \beta^{-2}\rho)u) + \mathrm{Div}_x((n + \beta^{-2}\rho)u \otimes u) + \nabla_x(p(n) + \rho) + (\eta n + \varsigma \rho)\nabla_x \Phi = 0, \tag{9}$$

whereas ρ and n are both advected by the velocity u:

$$\partial_t \rho + \nabla_x \cdot (\rho u) = 0 = \partial_t n + \nabla_x \cdot (n u). \tag{10}$$

3. Asymptotic preserving numerical methods

3.1. Bubbling regime

Our numerical strategy is based on the Hilbert expansion method which allows to guess the asymptotic behavior of the system (1). It suggests that

$$f_\epsilon(t,x,\xi) = \rho_\epsilon(t,x) M(\xi) + \sqrt{\epsilon} r_\epsilon(t,x,\xi) \tag{11}$$

where the remainder r_ϵ is expected to remain bounded (see Proposition 1). Furthermore, f_ϵ, r_ϵ satisfy

$$\partial_t f_\epsilon + \xi \cdot \nabla_x r_\epsilon + (u_\epsilon + \nabla_x \Phi) \cdot \nabla_\xi r_\epsilon = \frac{1}{\epsilon} L f_\epsilon + \frac{1}{\sqrt{\epsilon}} M(\xi) S_\epsilon(t,x,\xi), \tag{12}$$

where

$$S_\epsilon(t,x,\xi) = -\xi \cdot \nabla_x \rho_\epsilon - \xi \cdot (u_\epsilon(t,x) + \nabla_x \Phi)\rho_\epsilon,$$

and the evolution of the remainder obeys

$$\partial_t r_\epsilon = \frac{1}{\epsilon} L r_\epsilon + \frac{1}{\epsilon} M S_\epsilon - \frac{1}{\sqrt{\epsilon}} \left[\xi \cdot \nabla_x r_\epsilon + (u_\epsilon + \nabla_x \Phi) \nabla_\xi r_\epsilon - M \nabla_x \cdot \left(\int_{\mathbb{R}^3} \xi_\star r_\epsilon \, \mathrm{d}\xi_\star \right) \right]. \tag{13}$$

To derive the numerical scheme, we use a splitting algorithm to compute the evolution of both the density f_ϵ and its fluctuations r_ϵ by using relations (12) and (13) where we get rid in the right hand side of the lower order terms. This leads to the following scheme:

Given $n^k,\ u^k,\ f^k,\ r^k$, approximation of n, u, f, r at time $k\Delta t$,

- *Step 0:* Solve the Euler equations for the fluid density n and velocity u. We treat the source term explicitly so it reads

$$\int_{\mathbb{R}^3} \xi r^k \, \mathrm{d}\xi - u^k \int_{\mathbb{R}^3} f^k \, \mathrm{d}\xi.$$

We use a numerical method which preserves with accuracy the shock structure of the hyperbolic system, applying directly the scheme designed in [35,12–14,34,11]. This defines n^{k+1} and u^{k+1}.

Actually, since the limit equation for the density of particles is of parabolic type, it has a different typical time scale than those of the Euler equation; in turn, the equations involve different stability conditions. Hence, we perform Step 0 on a time interval $(k\Delta t_h, (k+1)\Delta t_h)$, and then we make several sub-cycles (Step 1–Step 2) below on time intervals $(k'\Delta t_p, (k'+1)\Delta t_p)$, for some $\Delta t_p < \Delta t_h$ (typically, the space mesh size Δx being given, we have $\Delta t_p = \mathcal{O}(\Delta x^2)$ but $\Delta t_h = \mathcal{O}(\Delta x)$).

- *Step 1:* Solve the stiff equations

$$\partial_t f = \frac{1}{\epsilon} L f, \quad \partial_t r = \frac{1}{\epsilon} L r + \frac{1}{\epsilon} M S,$$

where

$$S = -\xi \cdot \nabla_x \rho + \xi \cdot (u^{k+1} + \nabla_x \Phi)\rho,$$

getting rid of terms of order $\mathcal{O}(1/\sqrt{\epsilon})$ in (12) and (13), we will discuss these terms below. The crucial point is that $\rho = \int f \, \mathrm{d}\xi$ is not modified by the first equation: $\rho^{k'+1/2} = \int f^{k'+1/2} \, \mathrm{d}\xi = \rho^k$ so that the source term in the second equation can be treated as constant in time. Accordingly, we get

$$\begin{cases} f^{k'+1/2} = \mathrm{e}^{\Delta t L/\epsilon} f^{k'}, \\ r^{k'+1/2} = \mathrm{e}^{\Delta t L/\epsilon} r^{k'} + (1 - \mathrm{e}^{\Delta t L/\epsilon}) M S^{k'}. \end{cases} \tag{14}$$

- *Step 2.* Solve the transport-like part

$$\partial_t f + \xi \cdot \nabla_x r + (u^{k+1} + \nabla_x \Phi) \cdot \nabla_\xi r = 0, \quad \partial_t r = 0$$

(note that the convection term is of characteristic speed ξ and not $\xi/\sqrt{\epsilon}$) which defines $f^{k'+1}$ and $\rho^{k'+1} = \int f^{k'+1}\,\mathrm{d}\xi$.

This kind of asymptotic-induced schemes have been introduced by Klar [33,32], and, in a different version by Jin–Pareschi–Toscani [30,31], and revisited in [8,23]. The situation looks more complicated here since it involves the operator e^{tL}. This is what we detail now. We keep a fully explicit approach, using the fact that solutions of

$$\partial_t F = \frac{1}{\epsilon} LF + H$$

can be explicitly computed, see for instance [9], with a formula involving the fundamental solution

$$\mathcal{G}(t,\xi,\xi_\star) = \frac{1}{(2\pi(1-\delta(t)^2))^{N/2}} \exp\left(-\frac{|\,\xi - \delta(t)\xi_\star|^2}{2(1-\delta(t)^2)}\right), \quad \delta(t) = \mathrm{e}^{-t}$$

associated to the Fokker–Planck operator in dimension N. Hence, given a data $F(s,\xi)$, and a source term $H(\sigma,\xi)$, we get the Duhamel formula

$$\begin{aligned} F(t,\xi) &= \mathrm{e}^{(t-s)L/\epsilon} F(s,\xi) + \int_s^t \mathrm{e}^{(t-\sigma)L/\epsilon} H(\sigma,\xi)\,\mathrm{d}\sigma \\ &= \int_{\mathbb{R}^N} \mathcal{G}\Big(\frac{t-s}{\epsilon},\xi,\xi_\star\Big) F(s,\xi_\star)\mathrm{d}\xi_\star + \int_s^t \int_{\mathbb{R}^N} \mathcal{G}\Big(\frac{t-\sigma}{\epsilon},\xi,\xi_\star\Big) H(\sigma,\xi_\star)\mathrm{d}\xi_\star\,\mathrm{d}\sigma. \end{aligned}$$

These expressions involve the quantity $\mathrm{e}^{-t/\epsilon}$ with $0 < \epsilon \ll 1$, which motivates the use of the following expansion for $0 < \delta \ll 1$

$$D_\delta \int_{\mathbb{R}^N} \exp\left(-\frac{|\,\xi - \delta\xi_\star|^2}{2(1-\delta^2)}\right) F(\xi_\star)\mathrm{d}\xi_\star = M(\xi)\left(\int_{\mathbb{R}^N} F(\xi_\star)\mathrm{d}\xi_\star + \delta\xi \cdot \int_{\mathbb{R}^N} \xi_\star F(\xi_\star)\mathrm{d}\xi_\star\right) + \mathcal{O}(\delta^2).$$

with $D_\delta = (2\pi(1-\delta^2))^{-N/2}$. We use this expansion to approximate the Duhamel formula for $H(t,x,\xi) = \frac{1}{\epsilon} M(\xi) S((k'+1)\Delta t, x, \xi)$, which is not modified during the time step. Accordingly, we make the following identity appear

$$\frac{1}{\epsilon}\int_{k'\Delta t}^{(k'+1)\Delta t} \mathrm{e}^{(\sigma-(k'+1)\Delta t)/\epsilon}\,\mathrm{d}\sigma = 1 - \mathrm{e}^{-\Delta t/\epsilon}.$$

We are finally led to the following approximation for (14)

$$\begin{cases} f^{k'+1/2}(\xi) = M(\xi)\big(\rho^{k'} + \mathrm{e}^{-\Delta t/\epsilon}\xi \int_{\mathbb{R}^3} \xi_\star f^{k'}\,\mathrm{d}\xi_\star\big), \\ r^{k'+1/2}(\xi) = \mathrm{e}^{-\Delta t/\epsilon} M(\xi)\big(\xi \int_{\mathbb{R}^3} \xi_\star r^{k'}\,\mathrm{d}\xi_\star\big) + (1 - \mathrm{e}^{-\Delta t/\epsilon}) M(\xi) S^{k'}. \end{cases} \tag{15}$$

To obtain the second equation we used the fact that $\int_{\mathbb{R}^3} r^{k'}(\xi)\mathrm{d}\xi = 0$, and we keep in mind that $\rho^{k'+1/2} = \rho^{k'}$.

Remark 4. The terms of order $\mathcal{O}(1/\sqrt{\epsilon})$ in (12) and (13) can be disregarded due to this expansion. In fact, if we have kept them, we would have additional terms in the scheme of order $\mathcal{O}(\sqrt{\epsilon})$. For instance, in the equation for $f^{k'+1/2}(\xi)$, we should have an additional term coming from the approximation setting $H(t,x,\xi) = \frac{1}{\sqrt{\epsilon}} M(\xi) S((k'+1)\Delta t, x, \xi)$ which now leads to the additional term

$$\sqrt{\epsilon}(1 - \mathrm{e}^{-\Delta t/\epsilon}) M(\xi) S^{k'}.$$

Analogously, it happens with the additional term in the fluctuations. In fact, setting

$$H(t,x,\xi) = -\frac{1}{\sqrt{\epsilon}}\left[\xi \cdot \nabla_x r_\epsilon + (u_\epsilon + \nabla_x \Phi)\nabla_\xi r_\epsilon - M\nabla_x \cdot \left(\int_{\mathbb{R}^3} \xi_\star r_\epsilon\,\mathrm{d}\xi_\star\right)\right],$$

since its integral over ξ is zero, we obtain the additional term

$$\frac{1}{\sqrt{\epsilon}}M(\xi)\xi\cdot\int_{k'\Delta t}^{(k'+1)\Delta t} e^{(\sigma-(k'+1)\Delta t)/\epsilon}\int_{\mathbb{R}^3}\xi(\xi\cdot\nabla_x r_\epsilon)\mathrm{d}\xi\,\mathrm{d}\sigma \approx \sqrt{\epsilon}M(\xi)\xi\cdot\int_{\mathbb{R}^3}\xi(\xi\cdot\nabla_x r^{k'})\mathrm{d}\xi$$

that is disregarded.

Full discretization and mass conservation: The space and velocity discretizations deserve some comments since some care is needed to preserve the mass conservation observed at the continuous level. For the sake of clarity, we restrict the discussion to the one-dimension framework (which will be used for the simulations presented in the last Section). According to the approach in [23,8], we choose an upwind discretization for $\xi\partial_x r$ in Step 2 and a downwind discretization for $\xi\partial_x\rho$ in Step 1, so that we recover a centered scheme for the diffusion term in the limit $\epsilon\to 0$. For the discretization of $(u^{k+1}+\partial_x\Phi)\partial_\xi r$ in Step 2, we choose a centered discretization, in order to ensure the conservation of the total mass. To this end, we also prescribe for the convection Step 2 specular reflections for the fluxes associated to the convection in space, see [8] for similar conditions. To be more specific, we choose a *symmetric* space of $2M$ discrete velocities $\{\xi_1,\ldots,\xi_{2M}\}$ ranging from $-\xi_{\mathrm{Max}}$ to ξ_{Max} and we integrate through trapezoidal rule to ensure that the even moments of the odd functions in ξ vanish. Then, we write our fully discrete approximation of the x-derivative of r as

$$[\xi\partial_x r]_{j,m}\simeq\frac{\hat{g}_{j+1/2,m}-\hat{g}_{j-1/2,m}}{\Delta x},$$

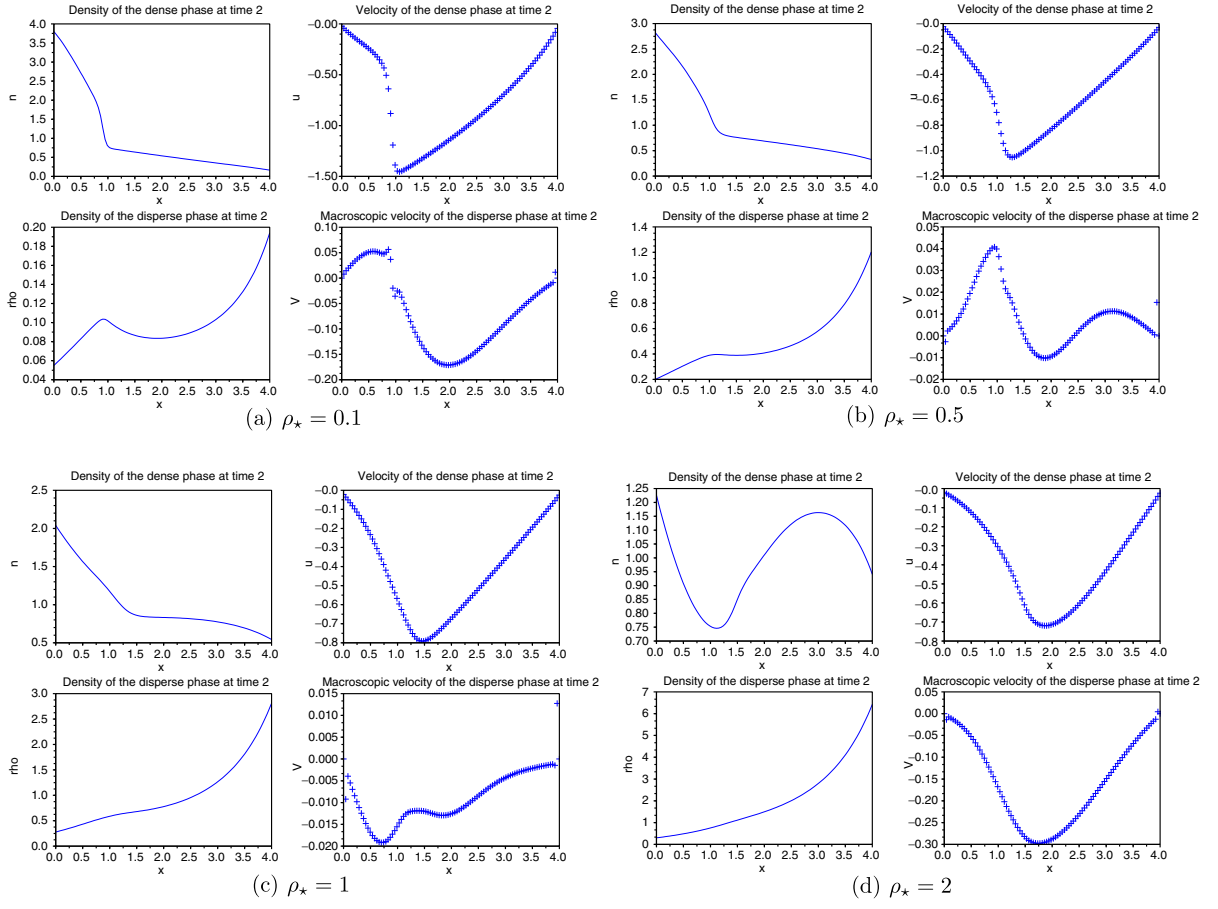

Fig. 1. Bubbling regime: simulation with $\epsilon=0$, $\gamma=1.4$, $F=1$ at time $T=2$. Comparison of the densities and velocities of particles, and of the dense phase for several $\rho_\star$. For this run $\xi_{\mathrm{Max}}=10$, $\Delta\xi=0.2$, $\Delta x=0.04$.

with $j \in \{1,\dots,J\}$ the discrete space index and $m \in \{1,\dots,2M\}$ the discrete velocity index, where due to the choice of upwinding, we have

$$\hat{g}_{j+1/2,m} = \begin{cases} \xi_m r_{j,m} & \text{if } \xi_m > 0, \\ \xi_m r_{j+1,m} & \text{if } \xi_m < 0. \end{cases}$$

For the boundary terms, we impose

$$\begin{cases} \hat{g}_{3/2,m} = -\hat{g}_{3/2,-m} & \text{if } \xi_m > 0, \\ \hat{g}_{J-1/2,m} = -\hat{g}_{J-1/2,-m} & \text{if } \xi_m < 0, \end{cases}$$

where $J-1$ is the number of intervals in the space variable labelled from 1 to $J-1$. For f, we choose a specular boundary condition at the end of Step 2:

$$\begin{cases} f_{1,m} = f_{2,-m} & \text{if } \xi_m > 0, \\ f_{J,m} = f_{J,-m} & \text{if } \xi_m < 0. \end{cases}$$

Moreover, at the end of Step 1, we impose a boundary condition on the fluctuations coherent with specular reflection for f. The specular reflection for f implies, due to the expansion $f = \rho M(\xi) + \sqrt{\epsilon} r$, specular reflection for r, or in other words, r must be an even function of ξ. Since at the end of Step 1 the fluctuation r is an odd

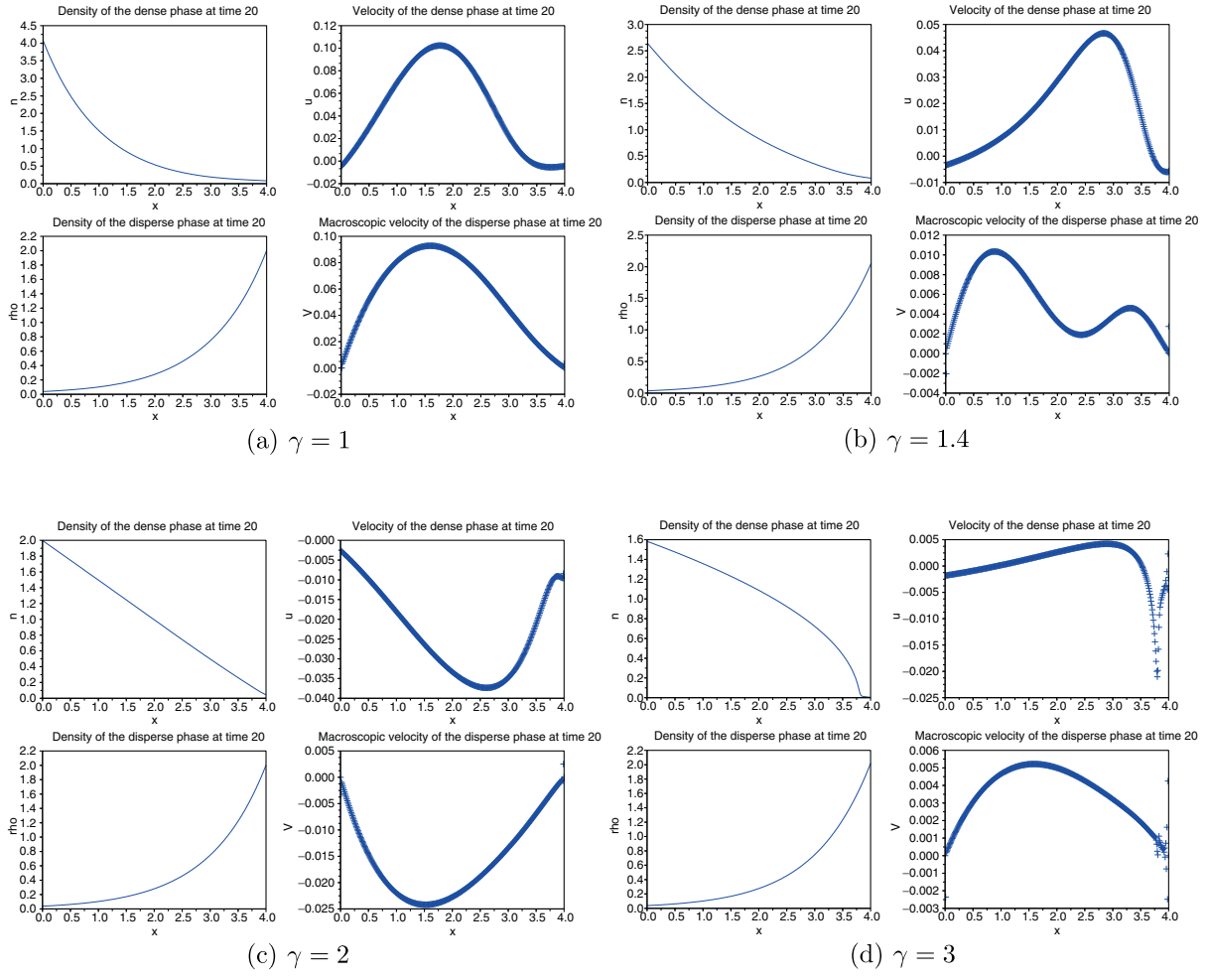

Fig. 2. Bubbling regime: simulation with $\epsilon = 0$, $\rho_\star = 0.5$, $F = 1$ at time $T = 20$. Comparison of the densities and velocities of particles, and of the dense phase for several γ. For this run $\xi_{\text{Max}} = 10$, $\Delta\xi = 0.2$, $\Delta x = 0.04$.

function of ξ, then r must vanish at the boundary. Thus $r = 0$ is imposed at the boundaries 2 and $J - 1$ implying finally, that $\hat{g}_{3/2,m} = \hat{g}_{J-1/2,m} = 0$ for all m. We also note that this numerical boundary condition exactly coincides when $\epsilon = 0$ with the discrete version of the Robin boundary condition (7) as in [8].

Asymptotic preserving: It is worth writing what the scheme does for $\epsilon = 0$. Formulae (15) become

$$\begin{cases} f^{k'+1/2}(\xi) = M(\xi)\int_{\mathbb{R}^3}[f^{k'+1/2} - \Delta t(\xi_\star \cdot \nabla_x + (u^{k+1} + \nabla_x \Phi) \cdot \nabla_\xi) r^{k'+1/2}]\mathrm{d}\xi_\star, \\ r^{k'+1/2}(\xi) = M(\xi) S^{k'} = M(\xi)[-\xi \cdot \nabla_x \rho^{k'} + \xi \cdot (u^{k+1} + \nabla_x \Phi)\rho^{k'}] \end{cases}$$

which coincide with the Hilbert expansion (11) and we recover the Smoluchowski equation, as expected. This means that the scheme is Asymptotic Preserving. Let us point out again that the derivation of the scheme is induced by the asymptotic regime: the method precisely aims at being relevant for small values of ϵ, when the presence of stiff terms make it definitely non affordable a direct computation of the original equation. We refer to [8] for such a discussion and examples. In particular, we checked that the scheme is consistent with the limit system when $\epsilon = 0$, and a further consistency analysis can be performed under the condition that ϵ tends to zero faster than Δt, in the spirit of [29]. Anyway, the approximation are intended to make the scheme valuable for a range of moderate positive values of ϵ.

Well balanced property: The equilibrium states for the kinetic equation read, up to a normalization factor, $e^{\Phi(x)}e^{-\xi^2/2}$. Of course, Step 1 does not modify such a distribution since it belongs to the kernel of the operator

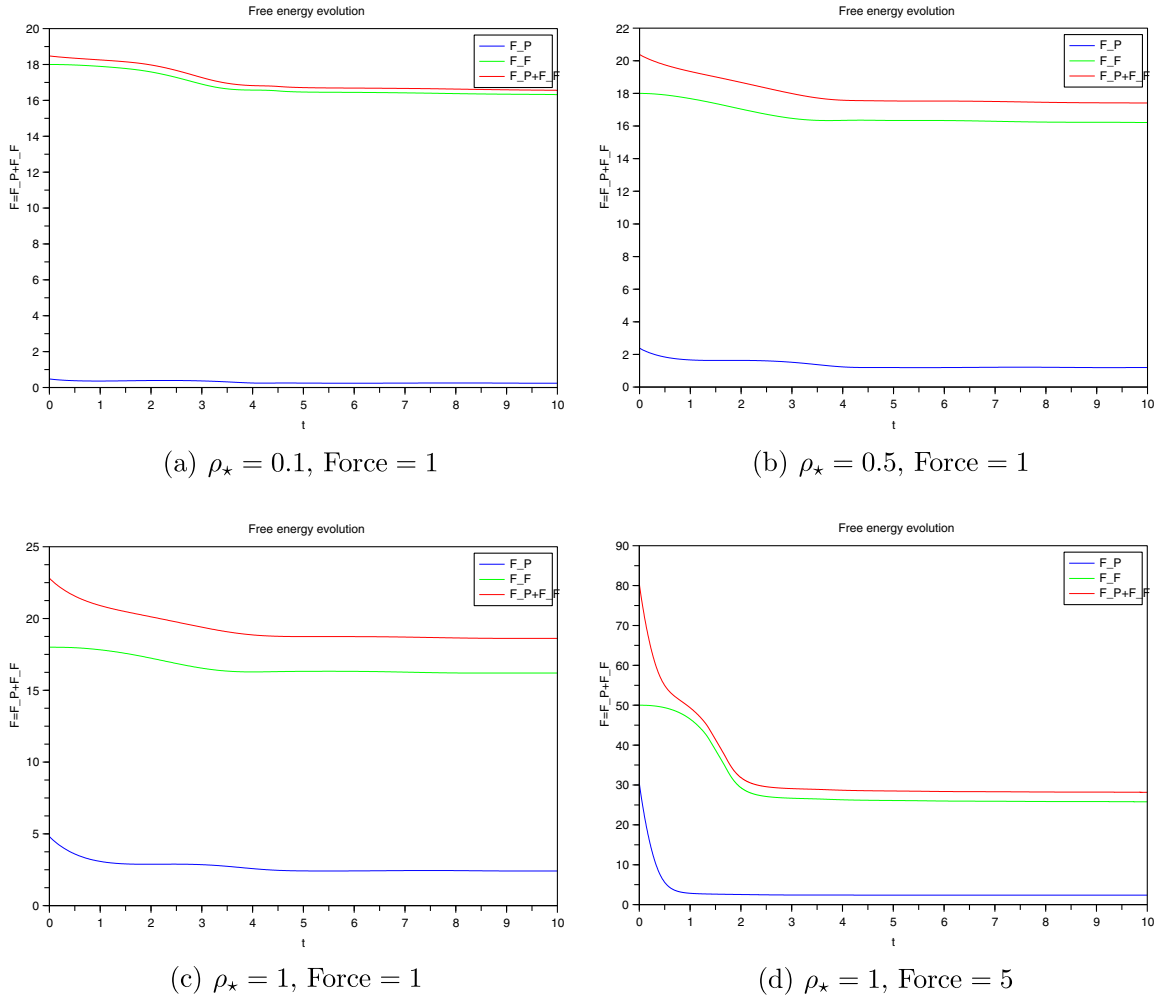

(a) $\rho_\star = 0.1$, Force $= 1$ (b) $\rho_\star = 0.5$, Force $= 1$

(c) $\rho_\star = 1$, Force $= 1$ (d) $\rho_\star = 1$, Force $= 5$

Fig. 3. Bubbling regime: evolution of the free energy ($\epsilon = 0$). For this run $\xi_{\mathrm{Max}} = 10$, $\Delta\xi = 0.2$, $\Delta x = 0.04$.

L. We rewrite $\partial_x \Phi \partial_\xi f = \frac{1}{\xi}(\xi \partial_x \Phi)\partial_\xi f$ which leads to the numerical approximation (upwind in space, centered in velocity)

$$\frac{1}{\xi_m}\frac{\xi_m}{\Delta x}(\Phi_j - \Phi_{j-1})\frac{f_{j,m+1} - f_{j,m-1}}{2\Delta\xi} \quad \text{if } \xi_m > 0,$$
$$\frac{1}{\xi_m}\frac{\xi_m}{\Delta x}(\Phi_{j+1} - \Phi_j)\frac{f_{j,m+1} - f_{j,m-1}}{2\Delta\xi} \quad \text{if } \xi_m < 0.$$

Applying the discrete operator approaching $\xi\partial_x + \partial_x\Phi\partial_\xi$ to the equilibrium state and using a Taylor expansion leads to an expression involving only odd powers of ξ_m (and thus a $\mathcal{O}(\Delta\xi^2)$ consistency error); in turn, using the symmetry of the set of discrete velocities, its average vanishes. This motivates the choice of a centered discretization for computing the derivative with respect to ξ. Similar considerations hold when we change the sign of the force term in the kinetic equation.

3.2. Flowing regime

We need another numerical strategy to deal with the flowing regime. It is much more delicate due to the presence of a stiff term in the Euler equation; furthermore, the limit system (9) and (10) is hyperbolic and does not involve any diffusive regularizing term. The scheme is based on the expansion

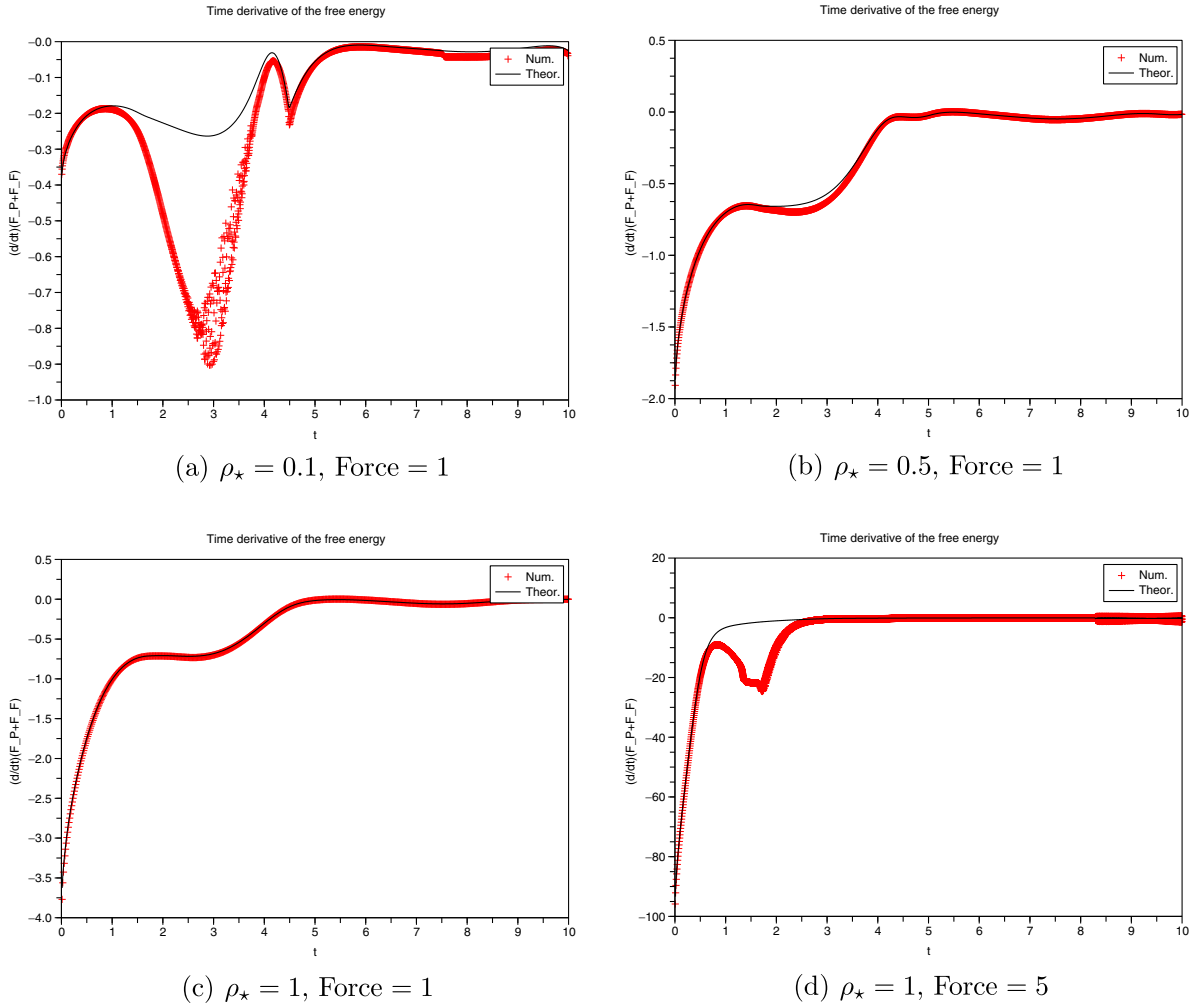

(a) $\rho_\star = 0.1$, Force $= 1$ (b) $\rho_\star = 0.5$, Force $= 1$

(c) $\rho_\star = 1$, Force $= 1$ (d) $\rho_\star = 1$, Force $= 5$

Fig. 4. Bubbling regime: evolution of the free energy ($\epsilon = 0$). For this run $\xi_{\text{Max}} = 10$, $\Delta\xi = 0.2$, $\Delta x = 0.04$.

$$f(t,x,\xi) = \rho(t,x) M_{u(t,x)/\beta}(\xi) + \epsilon r(t,x,\xi).$$

Note that this ansatz imposes that the size of the (rescaled) velocity u/β does not grow too much, so that it always remains well inside the (finite!) velocity grid, e.g for the one-dimension case in a given interval $[-\xi_{\mathrm{Max}}, +\xi_{\mathrm{Max}}]$. Otherwise, one would need to redefine this grid and follow the growth of the fluid velocity, leading to quite complicated interpolation procedures. The scheme is based on (8) which gives a way to compute the macroscopic friction force so that we get rid of the division by ϵ. The scheme works as follows.

Given (n^k, u^k, f^k), approximating n, u, f at time $k\Delta t$,

- *Step 0:* Solve the Euler equations for the fluid density n and velocity u. Assuming that the density of particles ρ remains constant during this time step, we use Després–Lagoutière's scheme to solve

$$\begin{cases} \partial_t n + \nabla_x \cdot (nu) = 0, \\ \partial_t (nu) + \mathrm{Div}_x (nu \otimes u) + \nabla p(n) + \eta n \nabla_x \Phi = -\frac{1}{\beta}\frac{1}{\Delta t}\left(\int \xi f^k \,\mathrm{d}\xi - \int \xi f^{k-1}\,\mathrm{d}\xi\right) \\ -\mathrm{Div}_x \int \xi \otimes \xi f^k \,\mathrm{d}\xi - \varsigma \nabla_x \Phi \int f^k \,\mathrm{d}\xi. \end{cases}$$

with reflection conditions for the velocity u. Let us point out that there is no boundary condition for n since the incoming flux vanishes at both ends. Then we cycle through the following (Step 1–Step 2) to get the time to t^{k+1}. Indeed, Step 0 is governed by a CFL condition based on the size of u which is supposed to remain far

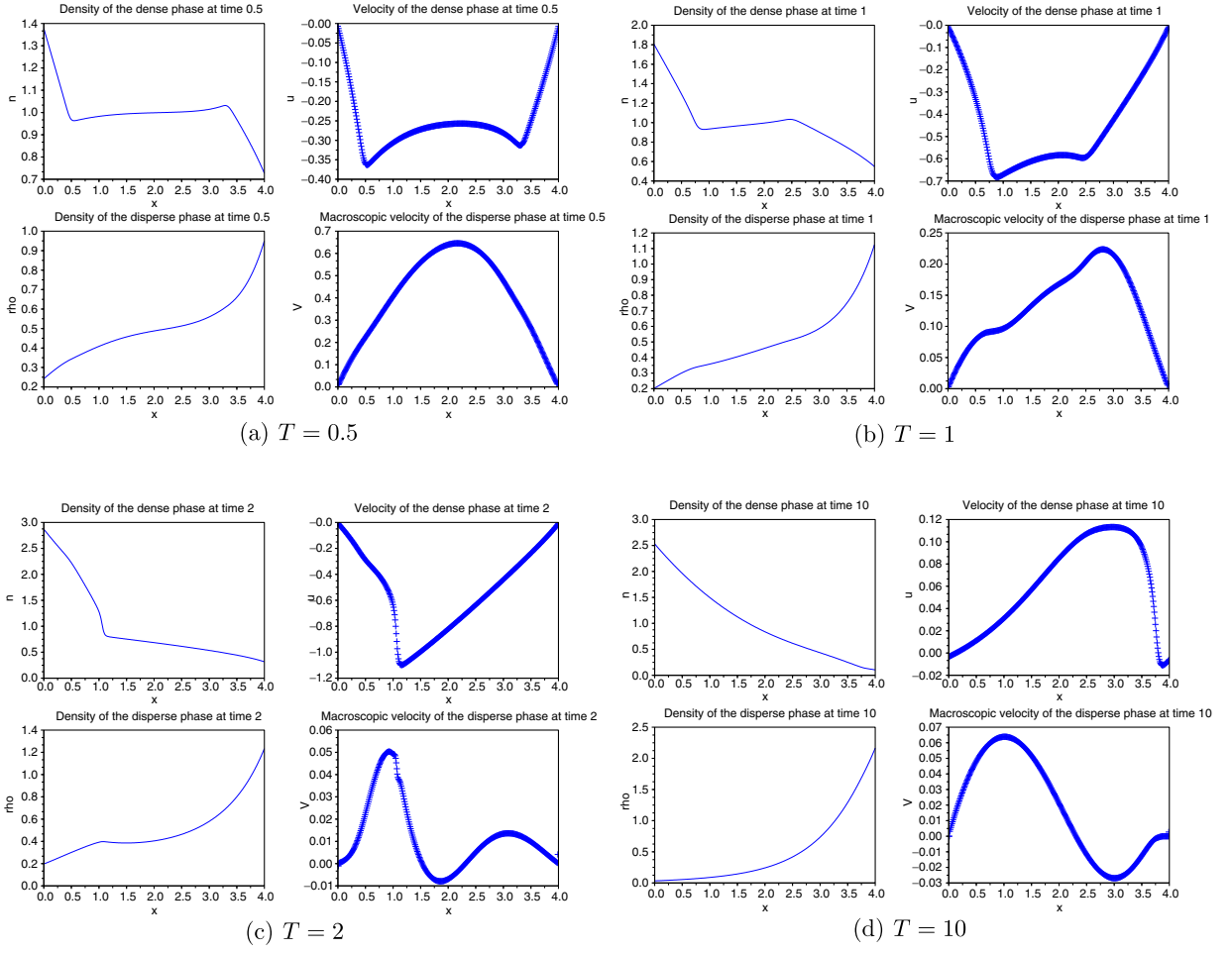

(a) $T = 0.5$ (b) $T = 1$

(c) $T = 2$ (d) $T = 10$

Fig. 5. Bubbling regime: evolution for $\epsilon = 0$, $F = 1$. For this run $\xi_{\mathrm{Max}} = 10$, $\Delta\xi = 0.2$, $\Delta x = 0.04$.

smaller than the largest microscopic velocity involved in the scheme; accordingly the time step imposed by the CFL associated to the advection terms in the kinetic equation is more constrained. Next, we compute the solution of the kinetic equation which enters in the definition of the source terms in the Euler system.

- *Step 1:* Solve the stiff equation

$$\partial_t f = \frac{1}{\epsilon} L_{u^{k+1}/\beta} f.$$

The macroscopic density $\rho = \int f \, d\xi$ is not modified during the time step so that $\rho^{k'+1/2} = \rho^{k'}$. According to the expansion of the kernel of the Fokker–Planck operator L_u, we thus define $f^{k'+1/2}$ by

$$f^{k'+1/2} = M_{u^{k+1}/\beta}\left[\int_{\mathbb{R}^3} f^{k'}(\xi_\star) d\xi_\star + e^{-\Delta t/\epsilon}(\xi - u^{k+1}/\beta)\int_{\mathbb{R}^3} (\xi_\star - u^{k+1}/\beta) f^{k'}(\xi_\star) d\xi_\star\right].$$

- *Step 2:* We solve the transport part of the kinetic equation

$$\partial_t f + \beta(\xi \cdot \nabla_x - \varsigma \nabla_x \Phi \cdot \nabla_\xi) f = 0$$

which defines $f^{k'+1}$ and $\rho^{k'+1} = \int f^{k'+1} \, d\xi$. As for the bubbling regime, we use a centered approximation to treat the derivative with respect to ξ, combined with a upwind approximation for the space derivatives of f and Φ.

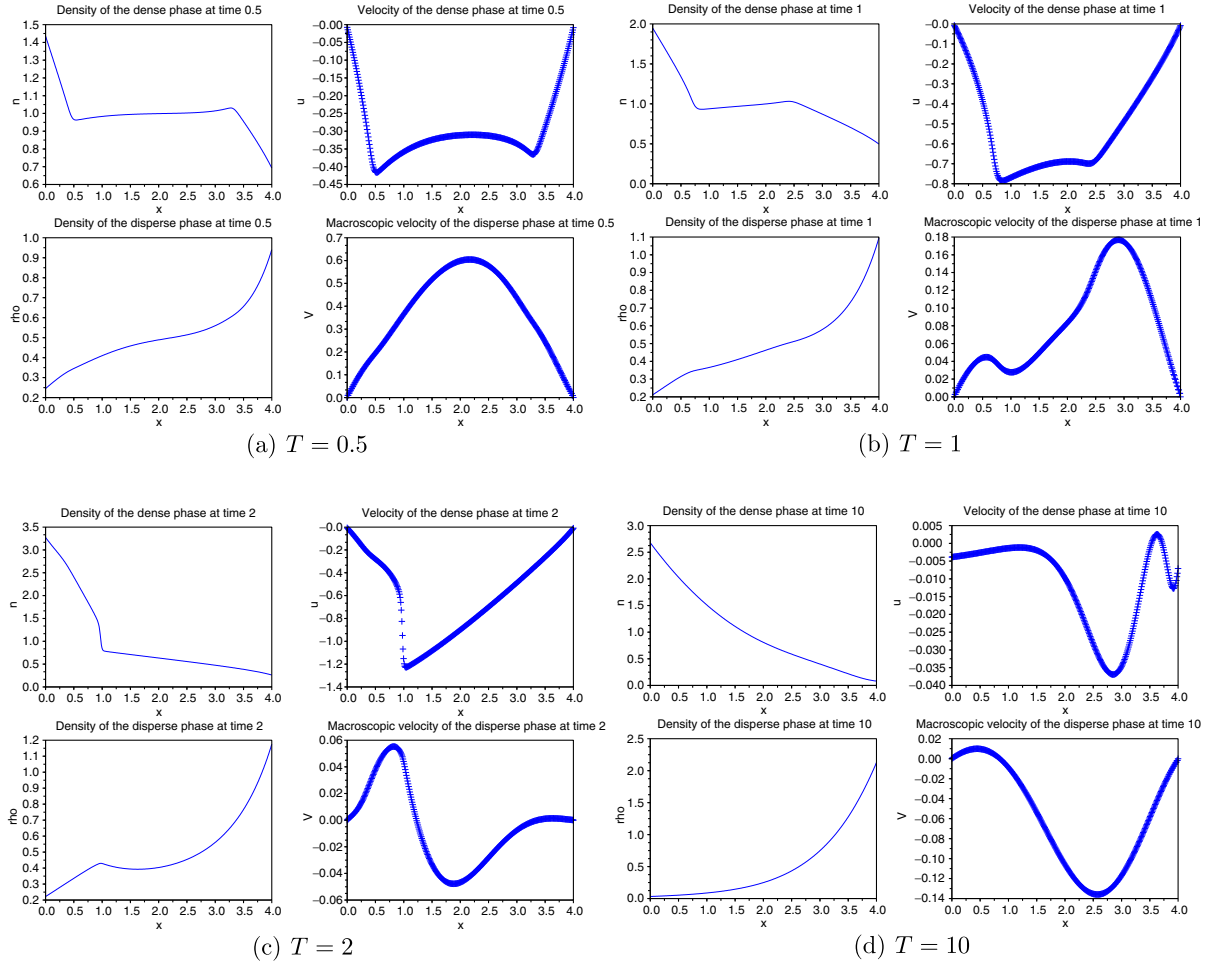

Fig. 6. Bubbling regime: evolution for $\epsilon = 0.1$, $F = 1$. For this run $\xi_{\text{Max}} = 10$, $\Delta\xi = 0.2$, $\Delta x = 0.04$.

Actually, due to the time derivative in the right hand side of the fluid system, we start with the kinetic part. We use a Strang approach: (Step 1–Step 2) is applied on a time step $\Delta t/2$, then we solve the hydrodynamic part Step 0 on a full time step Δt and go back to the kinetic equation. Again, the scheme is asymptotic preserving: for $\epsilon = 0$ we get $f = \rho M_{u/\beta}$ and integrating with respect to ξ leads to the limit system (9) and (10). Note that, in the spirit of the kinetic schemes for conservation laws [39], we do not use an evolution equation for the fluctuation, which makes the approach different from the one used for the bubbling regime. By the way, we emphasize that the schemes are really designed specifically for each asymptotic regime, and it is definitely hopeless to have in mind the use of one for the other.

4. Numerical experiments

For the numerical experiments, we restrict ourselves to the one-dimension framework (the computational domain being the slab $(0,4)$) with a force field, denoted by F, representing gravity and buoyancy effects. As mentioned in the Introduction, this case is particularly relevant when modeling the dispersion of pollutants emitted from ground sources [40]; it also applies to the description of thickening processes which are used in industrial procedures to separate suspensions into their solid and liquid parts [6].

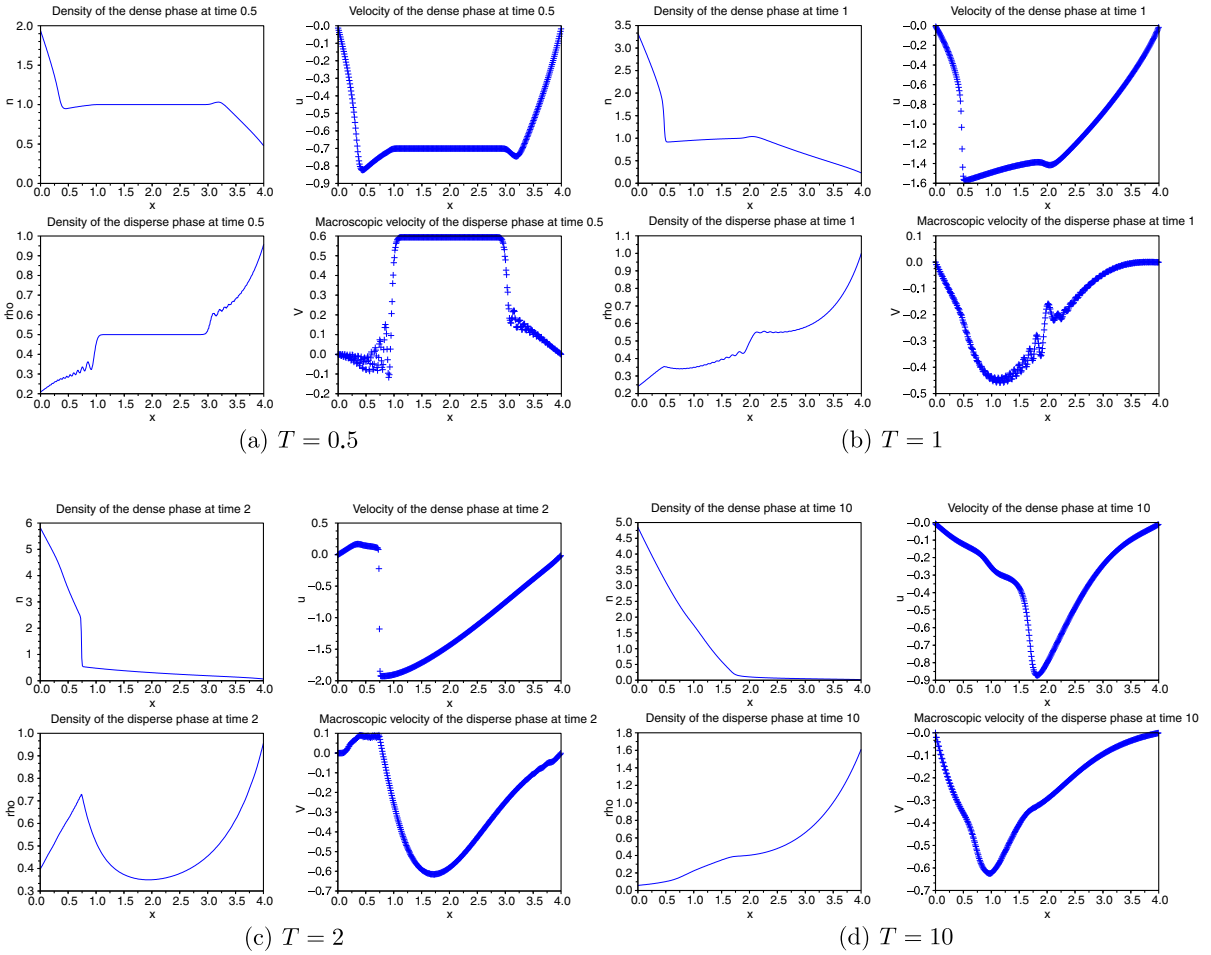

Fig. 7. Bubbling regime: evolution for $\epsilon = 0.5$, $F = 1$. For this run $\xi_{\mathrm{Max}} = 10$, $\Delta\xi = 0.2$, $\Delta x = 0.04$.

4.1. Bubbling regime

We show various simulations starting with the following data:

- The fluid is initially at rest $u(0,x) = 0$ with a uniform density $n(0,x) = 1$.
- The distribution function describing the particles is a centered Maxwellian with respect to velocity times a step function in space

$$f(0,x,\xi) = \rho_\star \mathbb{1}_{[a,b]}(x)\frac{e^{-\xi^2/2}}{\sqrt{2\pi}},$$

where $0 \leqslant a \leqslant b \leqslant 4$ and $\rho_\star$ is a positive constant.

In Fig. 1, we show the result at time $T = 2$ of the simulation where we make $\rho_\star$ vary with values 0.1, 0.5, 1 and 2, respectively. The smaller the concentration of particles, the faster the separation of the phases and the smoother the profiles of the velocities. At this time the sedimentation profile is clearly visible for $\rho_\star = 0.1$, with a front on the velocity of the dense phase. This shock coincides with a peak of the density for the particles which results from the friction force. As $\rho_\star$ increases these phenomena are not yet visible, but they will appear

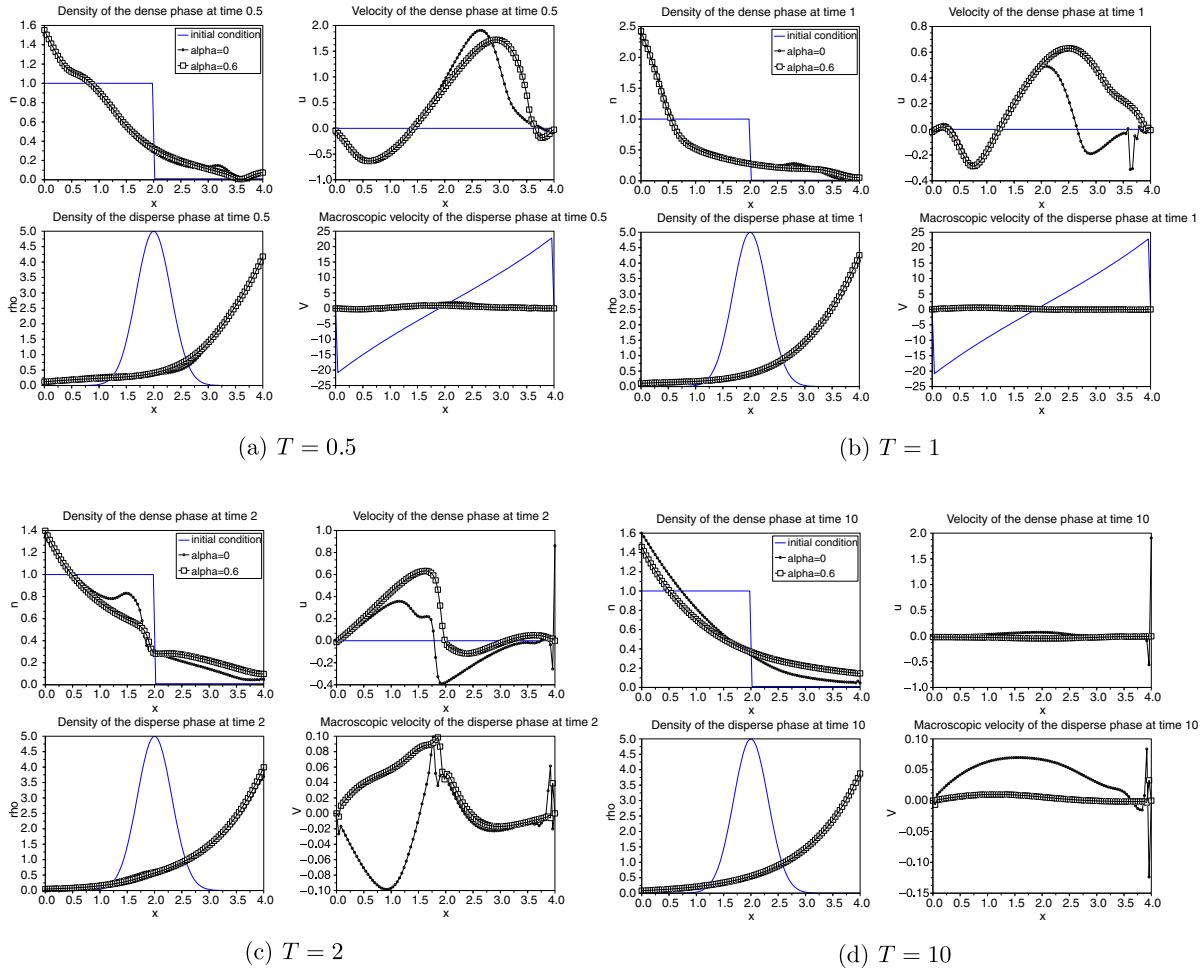

Fig. 8. Bubbling regime: comparison of the evolution for a constant fluid viscosity and a density-dependent viscosity, starting from an inhomogeneous fluid. Here, $\epsilon = 0$, $F = 1$, $\rho_\star = 5$, $\gamma = 1.4$. For this run $\xi_{\mathrm{Max}} = 10$, $\Delta\xi = 0.5$, $\Delta x = 0.04$.

at later times. Note that at this time, the velocity of the dense phase is negative, indicating a motion mainly driven by gravity. The difference as $\rho_\star$ varies agrees with the physical intuition: as $\rho_\star$ increases the friction with the particles slows down the fluid which in turn delays the phase separation.

Next, we investigate how the long time behavior depends on the pressure law. To this end, we start with the same configuration: $\rho_\star$ is 0.5 and we compute up to time $T = 20$ for several values of the adiabatic exponent. Results are displayed in Fig. 2. The shape of the density of the dense particles for large times depends on the pressure law, according to the stability results in [7]: the convexity of the profile changes at the critical value $\gamma = 2$ where it is linearly shaped, as expected from the results in [7]. Conversely, the final shape of the density of particles does not change significantly. We remark also that the velocity of the dense phase becomes small, an effect more sensible for the large values of γ.

It is remarkable that the scheme preserves the entropy dissipation property stated in Proposition 1. Indeed, Fig. 3 shows the evolution of $\mathcal{F}_\mathrm{P}$, $\mathcal{F}_\mathrm{F}$ and the total free energy $\mathcal{F}_\mathrm{P} + \mathcal{F}_\mathrm{F}$. We observe that the total energy decays with time, while the evolution of the free energy of the particles or of the fluid can be more involved. Fig. 4 shows the evolution of the entropy dissipation rate, which remains negative. It is computed in two different ways: either we compute the evolution of the (discrete) time derivative $\frac{\mathrm{d}}{\mathrm{d}t}(\mathcal{F}_\mathrm{P} + \mathcal{F}_\mathrm{F})$ (+-curve) or we compute directly the entropy dissipation term $\int \rho|\partial_x \Phi + \partial_x \ln \rho|^2 \,\mathrm{d}x$ (continuous curve), as given by the dissipation properties of the limit system, see [7]. A good agreement is obtained for the two computations, except in transient states: clearly the relative importance of the external force over the maximal density of particles has a

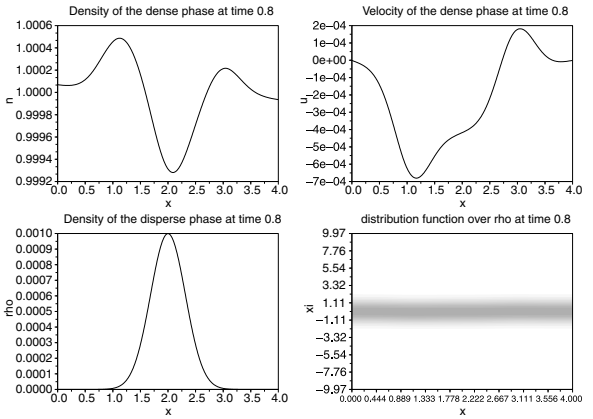

(a)

Therefore, the limit system as $\epsilon \to 0$ becomes

$$\begin{cases} \partial_t n + \mathrm{div}_x(nu) = 0, \\ \partial_t(nu) + \mathrm{div}_x(nu \otimes u) + \nabla_x p(n) + \eta_\star n \nabla_x \Phi = \frac{\rho \nabla_x \Phi - \nabla_x \rho}{n^\alpha}, \\ \partial_t \rho + \mathrm{div}_x(\rho u) = \mathrm{div}_x\left(\frac{\nabla_x \rho - \rho \nabla_x \Phi}{n^\alpha}\right). \end{cases}$$

In vacuum regions, formally the solution tends to satisfy $\rho = Ze^{-\Phi}$, with Z a normalization constant, and the right hand side of the momentum conservation equation vanishes. Note also that in the equation for ρ, we are faced with severe stability conditions, like $\Delta t/\Delta x^2 \leqslant 1/2 \min(n^\alpha/|\nabla_x \Phi|)$, in these regions of small density of the dense phase. The code is adapted as follows: (12) now reads

$$\partial_t f_\epsilon + \xi \cdot \nabla_x r_\epsilon + (n_\epsilon^\alpha u_\epsilon + \nabla_x \Phi) \cdot \nabla_\xi r_\epsilon = \frac{n_\epsilon^\alpha}{\epsilon} L f_\epsilon + \frac{1}{\sqrt{\epsilon}} M(\xi) S_\epsilon(t, x, \xi),$$

with

$$S_\epsilon(t, x, \xi) = -\xi \cdot \nabla_x \rho - \xi \cdot (n_\epsilon^\alpha u_\epsilon + \nabla_x \Phi) \rho_\epsilon.$$

Therefore, Step 1 of the algorithm is concerned with

$$\partial_t f = \frac{n_\epsilon^\alpha}{\epsilon} L f, \quad \partial_t r = \frac{n_\epsilon^\alpha}{\epsilon} L f + \frac{1}{\epsilon} M S$$

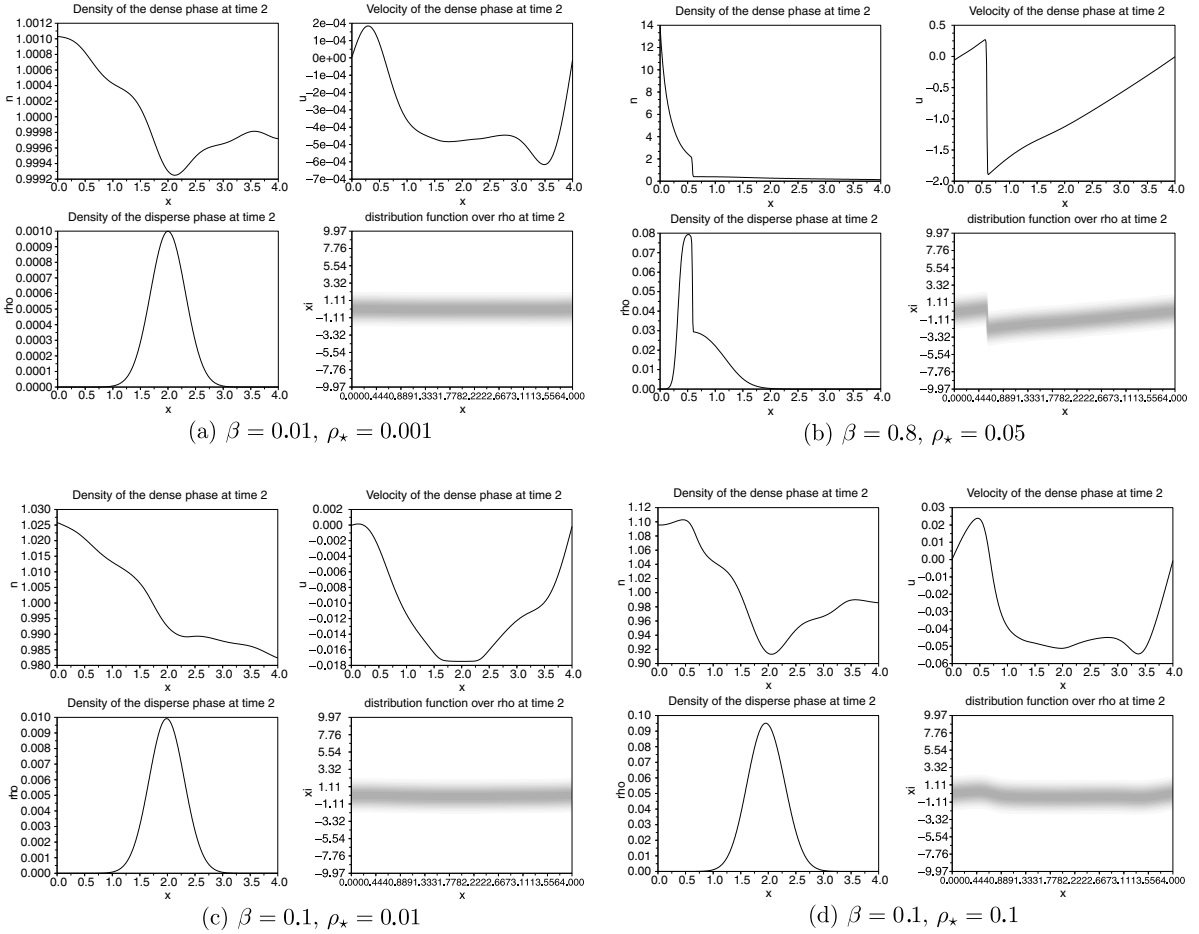

(a) $\beta = 0.01$, $\rho_\star = 0.001$ (b) $\beta = 0.8$, $\rho_\star = 0.05$

(c) $\beta = 0.1$, $\rho_\star = 0.01$ (d) $\beta = 0.1$, $\rho_\star = 0.1$

Fig. 11. Flowing regime: solution at time $T = 2$ for different values of β and $\rho_\star$. Here $\epsilon = 0.$, $F = 1$, $\gamma = 1.4$. For this run $\xi_{\mathrm{Max}} = 10$, $\Delta\xi = 0.5$, $\Delta x = 0.04$.

4.2. Flowing regime

Our simulations are performed with the same kind of initial data than in the previous section, but a slight modification for the disperse phase: in order to avoid too brutal initial effects from the boundaries, we set

$$f(0,x,\xi) = \rho_\star \mathrm{e}^{-10(x-2)^2/2} \frac{\mathrm{e}^{-\xi^2/2}}{\sqrt{2\pi}}.$$

Of course, simulating the equation with a small value of β is particularly tough since it produces a stiff term, $\beta^{-2}\partial_t J \simeq \beta^{-2}\partial_t(\rho u)$, in the momentum equation in Step 0 of the scheme. Keep in mind that with our scaling assumption this also means that $\rho_F \ll \rho_P$ (which is the typical situation for combustion applications). Note that performing formally $\beta \to 0$ in the limit system (9) and (10) leads to the pressureless gases system! However, in our simulations it turns out that the value of $\rho_\star$ has a strong influence on the behavior of the solution and the difficulty of the numerical simulation. In particular, there is a complex interplay between β and $\rho_\star$: working with smaller values of $\rho_\star$ allows to deal with small values of β before the oscillations appear in the computed quantities. At the beginning the particles act as a wall for the fluid, with a clear separation of the domain, especially when $\rho_\star$ is not small. Besides, the shape of the particles distribution does not seem to be affected by the motion of the fluid during the first times. This is particularly clear in Fig. 9, where both the values of β and $\rho_\star$ are small. Increasing the parameters might lead to a more involved behavior, as shown in Fig. 10. Considering later times, we observe a stronger influence on the particles density, as in Figs. 11 and 12. It is remarkable that the scheme reproduces brutal variations of the velocity. The particle density might also present some peaks, associated to the fronts of the density of the dense phase, and also to abrupt variations of the velocity, going from positive to negative values, see Figs. 11b and 12b–d. We also note that, while the pictures look very similar at earlier times, discrepancies appear for larger times, when dealing with several parameters: compare Fig. 9a, b and d with Fig. 11a, b and d. The code can be used to perform simulations for small values of positive ϵ as well but the main features remain essentially the same.

5. Conclusion

We introduce new numerical schemes specifically designed to handle asymptotic regimes for fluid–particles flows. A difficulty in our approach relies on the computation of the evolution semi-group associated to the Fokker–Planck operator, for which we propose a suitable approximation procedure, precisely based on the asymptotic regime we are interested in. Our scheme also includes a careful treatment of the boundary conditions which is required to preserve mass and to be consistent with the asymptotics. Here, we choose to apply the numerical strategy to simulate gravity/buoyancy driven flows. The schemes we propose are able to treat regimes of diffusive type and of hyperbolic type as well, and produce relevant results for a large range of the physical parameters.

Acknowledgement

The authors would like to thank Frédéric Lagoutière for several very fruitful discussions about this work. T.G. and P.L. thank the Centre de Recerca Matemàtica, Barcelona, Catalonia for its warm hospitality. J.A.C. thanks INRIA for the invitation in Lille and the support from the Spanish DGI-MCYT/FEDER project MTM2005-08024. The authors acknowledge partial support of the bilateral project France–Spain HF2006-0198.

References

[1] A.A. Amsden, J.D. Ramshaw, P.J. O'Rourke, J.K. Dukowicz, KIVA: a computer program for two- and three-dimensional fluid flows with chemical reactions and fuel sprays, Technical Report, Los Alamos National Laboratory, LA-10245-MS, 1985.

[2] C. Baranger, L. Desvillettes, Coupling Euler and Vlasov equations in the context of sprays: local smooth solutions, J. Hyperbol. Differ. Eq. 3 (1) (2006) 1–26.

[3] C. Baranger, G. Baudin, L. Boudin, B. Després, F. Lagoutière, E. Lapébie, T. Takahashi, Liquid jet generation and break-up, in: S. Cordier, Th. Goudon, M. Gutnic, E. Sonnendrucker (Eds.), Numerical Methods for Hyperbolic and Kinetic Equations, IRMA Lectures in Mathematics and Theoretical Physics, vol. 7, EMS Publishing House, 2005.
[4] C. Baranger, L. Boudin, P.-E. Jabin, S. Mancini, A modeling of biospray for the upper airways, ESAIM: Proc. 14 (2005) 41–47.
[5] S. Berres, R. Bürger, E.M. Tory, Mathematical model and numerical simulation of the liquid fluidization of polydisperse solid particle mixtures, Comput. Visual Sci. 6 (2004) 67–74.
[6] R. Bürger, W.L. Wendland, F. Concha, Model equations for gravitational sedimentation–consolidation processes, Z. Angew. Math. Mech. 80 (2) (2000) 79–92.
[7] J.-A. Carrillo, Th. Goudon, Stability and asymptotics analysis of a fluid–particles interaction model, Commun. PDE 31 (2006) 1349–1379.
[8] J.-A. Carrillo, Th. Goudon, P. Lafitte, F. Vecil, Numerical schemes of diffusion asymptotics and moment closures for kinetic equations, J. Sci. Comput., in press.
[9] J.-A. Carrillo, G. Toscani, Exponential convergence toward equilibrium for homogeneous Fokker–Planck-type equations, Math. Methods Appl. Sci. 21 (1998) 1269–1286.
[10] R. Caflisch, G. Papanicolaou, Dynamic theory of suspensions with Brownian effects, SIAM J. Appl. Math. 43 (1983) 885–906.
[11] B. Després, F. Lagoutière, Un schéma non linéaire anti-dissipatif pour l'équation d'advection linéaire, CR Acad. Sci. Paris Sér. I Math. 328 (10) (1999) 939–944.
[12] B. Després, F. Lagoutière, Contact discontinuity capturing schemes for linear advection and compressible gas dynamics, J. Sci. Comput. 16 (4) (2002) 479–524 (2001).
[13] B. Després, F. Lagoutière, Generalized Harten formalism and longitudinal variation diminishing schemes for linear advection on arbitrary grids, M2AN Math. Model. Numer. Anal. 35 (6) (2001) 1159–1183.
[14] B. Després, F. Lagoutière, A longitudinal variation diminishing estimate for linear advection on arbitrary grids, CR Acad. Sci. Paris Sér. I Math. 332 (3) (2001) 259–263.
[15] K. Domelevo, P. Villedieu, A hierarchy of models for turbulent disperse two-phase flows derived from a kinetic equation for the joint particle-gas, Commun. Math. Sci. 5 (2007) 331–353.
[16] A. Einstein, On the motion of small particles suspended in liquids at rest required by the molecular-kinetic theory of heat, Ann. Phys. 17 (1905) 549–560.
[17] T. Elperin, N. Kleeorin, M.A. Liberman, V.S. LÕvov, A. Pomyalov, I. Rogachevskii. Clustering of fuel droplets and quality of spray in Diesel engines. <http://arxiv.org/nlin.CD/0305017v1>.
[18] G. Falkovich, A. Fouxon, M.G. Stepanov, Acceleration of rain initiation by cloud turbulence, Nature 219 (2002) 151–154.
[19] Gas Viscosity Calculator. <http://www.lmnoeng.com/Flow/GasViscosity.htm>.
[20] S. Gavrilyuck, V. Teshukhov, Kinetic model for the motion of compressible bubbles in a perfect fluid, Eur. J. Mech. B: Fluids 21 (2002) 469–491.
[21] Th. Goudon, P.-E. Jabin, A. Vasseur, Hydrodynamic limit for the Vlasov–Navier–Stokes equations. I. Light particles regime, Indiana Univ. Math. J. 53 (6) (2004) 1495–1515.
[22] Th. Goudon, P.-E. Jabin, A. Vasseur, Hydrodynamic limit for the Vlasov–Navier–Stokes equations. II. Fine particles regime, Indiana Univ. Math. J. 53 (6) (2004) 1517–1536.
[23] Th. Goudon, P. Lafitte, Splitting schemes for the simulation of non equilibrium radiative flows, preprint (2007).
[24] T. Goudon, F. Poupaud, On the modeling of the transport of particles in turbulent flows, M2AN Math. Model. Numer. Anal. 38 (2004) 673–690.
[25] K. Hamdache, Unpublished work, Personal communication, 1997.
[26] K. Hamdache, Global existence and large time behaviour of solutions for the Vlasov–Stokes equations, Jpn. J. Ind. Appl. Math. 15 (1998) 51–74.
[27] H. Herrero, B. Lucquin-Desreux, B. Perthame, On the motion of disperse balls in a potential flow: a kinetic description of the added mass effect, SIAM J. Appl. Math. 60 (1999) 61–83.
[28] P.-E. Jabin, B. Perthame, Notes on mathematical problems on the dynamics of disperse particles interacting through a fluid. In: Modeling in Applied Sciences, Model. Simul. Sci. Eng. Technol., Birkhäuser Boston, Boston, MA, 2000, pp. 111–147.
[29] S. Jin, Efficient asymptotic-preserving (AP) schemes for some multiscale kinetic equations, SIAM J. Sci. Comput. 21 (2) (1999) 441–454.
[30] S. Jin, L. Pareschi, G. Toscani, Diffusive relaxation schemes for discrete-velocity kinetic equations, SIAM J. Numer. Anal. 35 (1998) 2405–2439.
[31] S. Jin, L. Pareschi, G. Toscani, Uniformly accurate diffusive relaxation schemes for multiscale transport equations, SIAM J. Numer. Anal. 38 (2000) 913–936.
[32] A. Klar, An asymptotic-induced scheme for nonstationary transport equations in the diffusive limit, SIAM J. Numer. Anal. 35 (3) (1998) 073–1094, (electronic).
[33] A. Klar, An asymptotic preserving numerical scheme for kinetic equations in the low Mach number limit, SIAM J. Numer. Anal. 36 (5) (1999) 1507–1527, (electronic).
[34] F. Lagoutière, Numerical resolution of scalar convex equations: explicit stability, entropy and convergence conditions. In: CEMRACS 1999 (Orsay), ESAIM Proc., vol. 10, 1999, pp. 183–199.
[35] F. Lagoutière, A non-dissipative entropic scheme for convex scalar equations via discontinuous cell-reconstruction, CR Math. Acad. Sci. Paris 338 (7) (2004) 549–554.

[36] G. Lavergne, Modélisation de l'écoulement multiphasique dans le propulseur à poudre P230 d'Ariane 5, in: Lecture Notes of the School of the Groupement Français de Combustion, Ile d'Oléron, 2004.
[37] A. Mellet, A.Vasseur, Vasseur, Global weak solutions for a Vlasov–Fokker–Planck/Navier–Stokes system of equations, Math. Model. Method Appl. Sci. 17 (7) (2007) 1039–1063.
[38] A. Mellet, A. Vasseur, Asymptotic analysis for a Vlasov–Fokker–Planck/Compressible Navier–Stokes system of equations, Commun. Math. Phys., in press.
[39] B. Perthame, Kinetic Formulation of Conservation Laws, Lecture Series in Mathematics and its Applications, Oxford University Press, Oxford, 2003.
[40] I. Vinkovic, Dispersion et mélange turbulents de particules solides et de gouttelettes par une simulation des grandes échelles et une modélisation stochastique lagrangienne. Application à la pollution de l'atmosphère. Thèse de doctorat, Ecole Centrale de Lyon, 2005.
[41] F.A. Williams, Spray combustion and atomization, Phys. Fluid 1 (1958) 541–555.
[42] F.A. Williams, Combustion Theory, second ed., Benjamin Cummings Publishing, 1985.